Journal of the Optical Society of Korea
Vol. 13, No. 1, March 2009, pp. 139-145

DOI: 10.3807/JOSK.2009.13.1.139

Resolution-enhanced Reconstruction of 3D Object Using Depth-reversed Elemental Images for Partially Occluded Object Recognitionz

Tan-Chun Wei, Dong-Hak Shin*, and Byung-Gook Lee

Department of Visual Contents, Dongseo University, San 69-1, Jurye-2-Dong, Sasang-Gu, Busan 617-716, Korea

(Received September 25, 2008 : revised January 30, 2009 : accepted January 30, 2009)

Computational integral imaging (CII) is a new method for 3D imaging and visualization. However, it suffers from seriously poor image quality of the reconstructed image as the reconstructed image plane increases. In this paper, to overcome this problem, we propose a CII method based on a smart pixel mapping (SPM) technique for partially occluded 3D object recognition, in which the object to be recognized is located at far distance from the lenslet array. In the SPM-based CII, the use of SPM moves a far 3D object toward the near lenslet array and then improves the image quality of the reconstructed image. To show the usefulness of the proposed method, we carry out some experiments for occluded objects and present the experimental results.

Keywords: 3D display, Integral imaging, Computational reconstruction, Lenslet array

OCIS codes : (100.6890) Three-dimensional image processing; (110.6880) Three-dimensional image acquisition

I. INTRODUCTION

Integral imaging is a new method for 3D imaging and visualization using a lenslet array [1]. Compared to other 3D imaging and display techniques, integral imaging has some advantages including full parallax, continuous viewing points and color imaging. In general, an integral imaging system consists of two processes: pickup and reconstruction [2-5]. In the pickup process, a lenslet array is used to capture the 3D object. Each of the lenslets provides a different perspective view of a 3D object, which results in a collection of demagnified 2D images. The captured image is called an elemental image array (EIA). In the reconstruction process, 3D images are reconstructed in reverse from the EIA through a similar lenslet array used in the pickup process.

In integral imaging, the reconstruction process of the 3D image can be done either optically or computationally. Optical reconstruction tends to degrade the image quality due to the diffraction and limitation of optical devices. To overcome these problems, computational reconstruction was studied [6-11]. Computational reconstruction is a technique based on the ray-tracing analysis to simulate the ray propagation mechanism by using a computer. The 3D image reconstructed with this technique does not have the problems caused by optical reconstruction as there are no optical devices involved. However, computational reconstruction also suffers from a few drawbacks such as low resolution, high computational cost, and interference between elemental images [9]. Many methods have been studied to overcome these problems [7-11]. Recently, one of our authors proposed a reconstruction method using a digital depth-conversion method, which is called smart pixel mapping [12], for EIA to reduce the computational cost [13]. SPM is a digital mapping procedure to map the EIA to an image plane.

The SPM-based computational reconstruction may be useful for pattern recognition of partially occluded 3D objects [14,15], in which the 3D object to be recognized is always located much farther from the lenslet array compared to the occlusion. In fact, the previous computational reconstruction method suffers from seriously poor image quality of the reconstructed image as the reconstructed output plane increases. In other words,

*Corresponding author: shindh2@dongseo.ac.kr

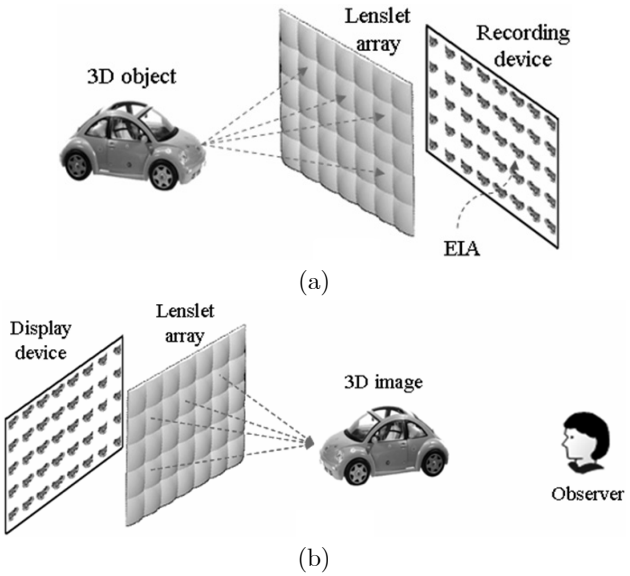

FIG. 1. Principle of integral imaging (a) pickup (b) display

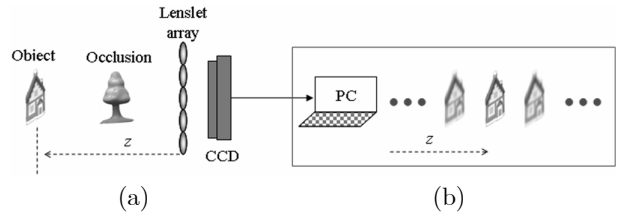

FIG. 2. Computational integral imaging (a) Pickup (b) CIIR process

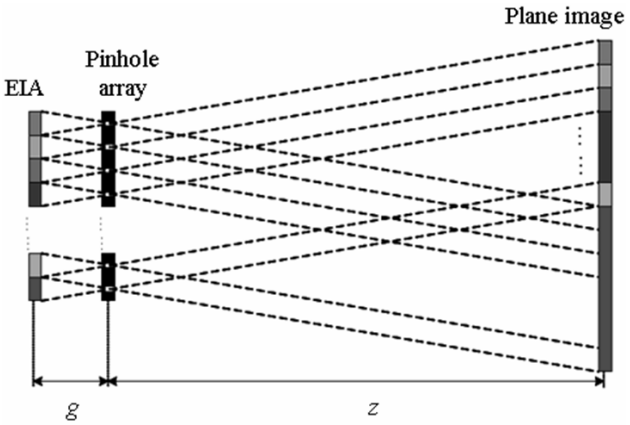

FIG. 3. Ray diagram of CIIR process

large depth of the reconstructed output plane requires a large magnification factor in the computational reconstruction processes so that many overlapping process increases interference noise among adjacent pixels in the reconstructed image. Therefore, if we reduce the distance of the output plane with the help of SPM, occluded 3D objects can be reconstructed to improve the resolution because the interference noise decreases in the reconstructed image.

In this paper, we apply SPM to the CII system for partially occluded 3D object reconstruction. Due to the use of the SPM technique, the originally recorded EIA is digitally mapped to an output plane to form a new EIA, which can be used to reverse the depth of 3D objects located farther from the lenslet array. The depth-reversed EIA allows the 3D image to be reconstructed at the distance near to the lenslet array, which implies the 3D image can be reconstructed with higher resolution.

II. REVIEW OF INTEGRAL IMAGING

Fundamentally, an integral imaging system consists of two processes: pickup and reconstruction, as shown in Fig. 1. In the pickup process as shown in Fig. 1(a), the rays coming from a 3D object through a pinhole array are recorded by use of a recording device as a form of two-dimensional (2D) EIA representing different perspectives of a 3D object. On the other hand, in the reconstruction process as shown in Fig. 1(b), the recorded EIA are displayed on a display panel and then the 3D image can be reconstructed and observed optically through a lenslet array.

On the other hand, the 3D image may be also computationally reconstructed from the optically recorded EIA. This system is called a computational integral imaging (CII) [14]. The general CII system is shown in Fig. 2. Compared to the integral imaging shown in Fig. 1, the reconstruction process is performed in a computer only. One of the popular computation reconstruction methods is a computational integral imaging reconstruction (CIIR). Figure 3 shows an operational principle of the CIIR technique based on a pinhole model [7]. First, an elemental image is projected inversely through the corresponding pinhole. Second, if an image is reconstructed on the output plane from the pinhole array, the inversely projected elemental image is digitally magnified by z/g, representing the ratio of the distance z between the virtual pinhole array and the reconstructed output plane to the distance g between the pinhole array and the elemental image plane. Third, the enlarged elemental image is overlapped and summed at the corresponding pixels of the reconstructed image plane along the z axis. To completely reconstruct a plane image of a 3D object at the distance of z, this same process must be repeatedly performed for all of the acquired EIA through each corresponding pinhole. Through iterative computation of the above process by increasing the z value, a series of z-dependent plane images can be reconstructed along the output plane.

Recently an analysis for the image degradation of the CIIR process has been reported [11]. The main reason for image degradation is that a large magnification causes interference among elemental images when they are superposed. The magnification factor largely depends on the distance of the reconstruction plane in CIIR. That

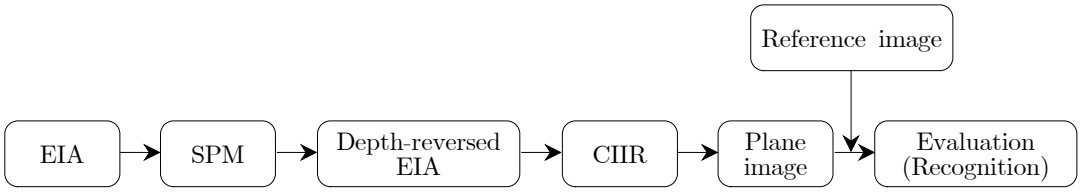

FIG. 4. Architecture of the proposed CII system

is, the magnification factor increases as the distance increases. Thus, a method to reduce the distance of the reconstruction plane can be considered as a good solution for this problem.

III. SPM-BASED CII FOR PARTIALLY OCCLUDED 3D OCJECT RECOGNITION

One of the popular applications of a CII system is the recognition of partially occluded 3D objects, in which occlusion seriously degrades system performance. The general system is shown in Fig. 2. Since the occlusion is located in front of a 3D object (target object) of interest, the EIA of partially occluded objects is recorded in the CCD camera. Then, in the CIIR process using the recorded EIA we can reconstruct a series of plane images along the output plane. The plane image of the target object is obtained at the far distance where it is originally located, as shown in Fig. 2(b). The reconstructed plane image of the occluded object is finally correlated with the original target object. The correlation performance depends on the resolution of reconstructed images.

In this paper, to improve the resolution of reconstruction images in the CIIR process, we apply the SPM technique to the CII system. The architecture of our SPM-based CII system is shown in Fig. 4. In our proposed CII system, the EIA for 3D objects consisting of occlusion and target object is optically recorded. Then we transform the depth of the original EIA by using the SPM technique, which will result in a new depth-reversed EIA. The depth-reversed EIA is applied in CIIR process and reconstructed as plane images. The final result is an output plane image which can be applied to the image evaluation or object recognition.

3.1 Smart Pixel Mapping

The principle of the SPM method is illustrated in Fig. 5. SPM is a computational depth-reverse process in which the original EIA is convertible to ones recorded at the different pickup distance [12]. As shown in Fig. 5, the EIA recorded at the far distance can be converted to one recorded near to the lenslet array. This effect can give us the movement of the output plane in the CIIR method for the target object as shown in Fig. 5. By using this effect, we can obtain the resolution-enhanced plane image by reducing the interference problem from the magnification process.

The depth conversion in SPM involves a two-step recording process. In the first step, the 3D objects are recorded as the first EIA. By using the recorded EIA, 3D images are reconstructed at the distance at which it was captured. The reconstructed 3D images are then recorded again by a similar virtual pickup system to produce a depth-reversed EIA. Here SPM is implemented using a direct pixels mapping process by using the first recorded EIA denoted by F. The conversion process is done digitally to produce the second set of EIA. The SPM algorithm for 1D case is formulated as

$$T_m^n = F_k^l \tag{1}$$

where

$$l = (N+1) - n \tag{2}$$

and

$$k = \begin{cases} m + M/2 - n & \text{if } M \text{ is even} \\ m + (M+1)/2 - n & \text{if } M \text{ is odd} \end{cases} \tag{3}$$

In Eq. (1), T is the output of F after applying the SPM. The subscripts m and k are corresponding to the elemental image number and n and l are the pixel number in the given elemental image, respectively. The values M and N are the total number of EIA and the total pixels per elemental image, respectively. We set T equals to zero if the corresponding $k < 1$ or $k > M$. The effective distance of SPM is given as

$$d = M \times g \tag{4}$$

where g is the distance between lenslet array and EIA.

3.2 CIIR PROCESS

The concept of CIIR can be explained by using Fig. 5(b). Let the (p,q)-th elemental image be E_{pq}. In order to reconstruct a plane image, elemental images inversely mapped to an output plane located at longitudinal distance z. The mapped elemental images on the output plane are magnified by applying a magnification factor. Then, the inverse mapped image R_{pq}^z of E_{pq} at the distance z is written as

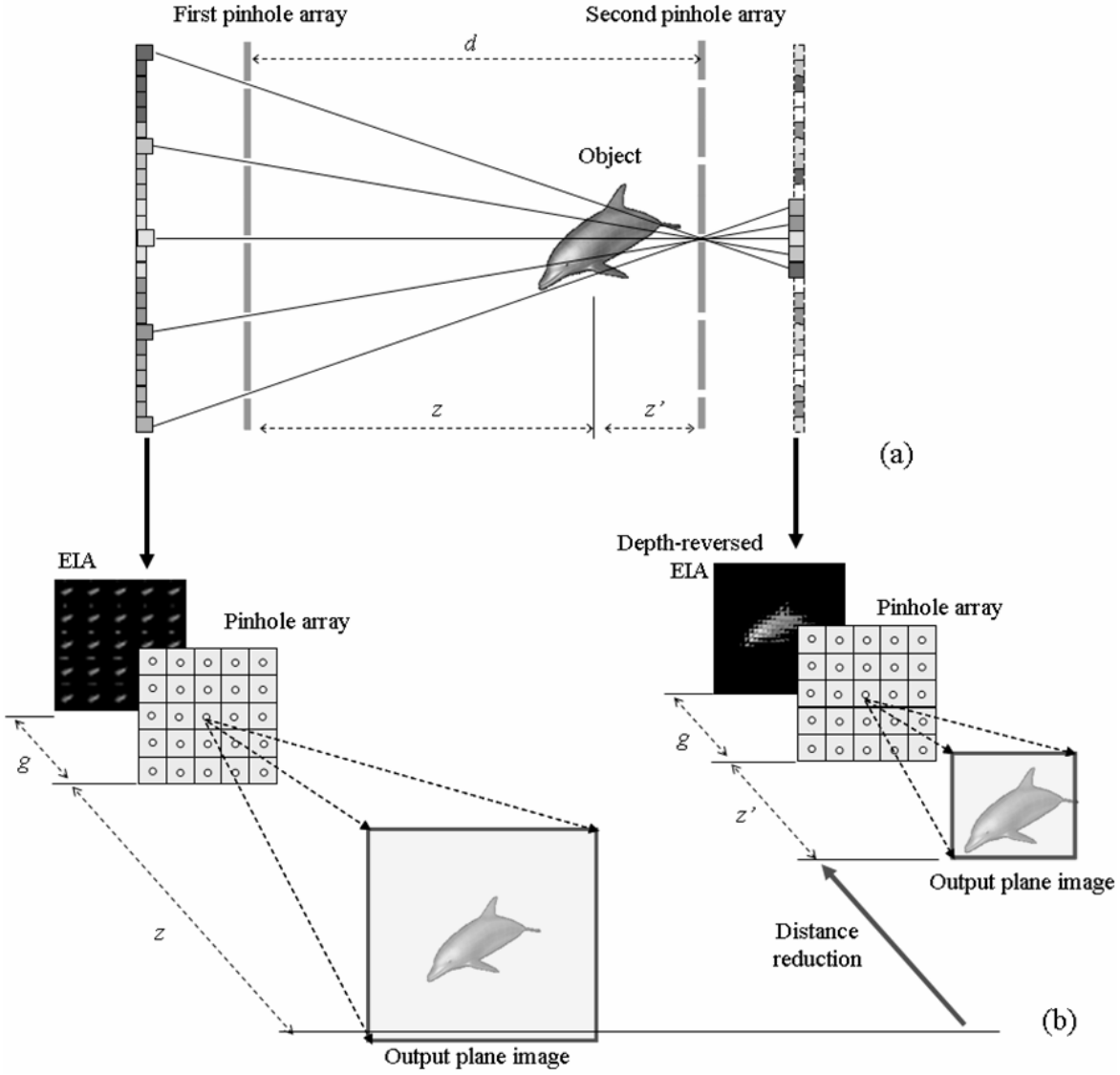

FIG. 5. (a) Ray mapping for SPM. (b) Example of CIIR reconstruction using the original EIA and the depth-reversed EIA.

$$R_{pq}^{z}(x,y)=\left(\frac{g}{z}\right)^{2}E\left(\frac{-gx}{z}+\left(1+\frac{g}{z}\right)s_{x}P,\frac{-gy}{z}+\left(1+\frac{g}{z}\right)s_{x}q\right)$$

$$\text{for}\quad\begin{cases}s_{x}(p-z/2g\le x\le s_{x}(p+z/2g)\\ s_{y}(q-z/2g\le y\le s_{y}(q+z/2g)\end{cases}\tag{5}$$

where the s_x and s_y are the size of an elemental image in x and y directions, respectively. The reconstructed plane image $R^z(x,y)$ at the output plane z can be expressed as the summation of all the inversely mapped elemental images and given by

$$R^{z}(x,y)=\sum_{p=0}^{m-1}\sum_{q=0}^{n-1}R_{pq}^{z}(x,y)\tag{6}$$

where m and n indicate the number of elemental images in x and y directions, respectively. Due to the magnification for each inversely mapped elemental image, superposition occurs for $z/g>1$. And the overlapping numbers of inversely mapped elemental images to reconstruct a certain pixel may be different from the corresponding numbers used to reconstruct the adjacent pixels. These variations in intensity generate the degradation of the quality of the reconstructed images. Therefore the compensation process is required. To do so, we count the overlapping number $N^z(x,y)$ for each pixel. The normalized plane image is given by

$$R_{normal}^{z}(x,y)=\frac{R^{z}(x,y)}{N^{z}(x,y)}\tag{7}$$

As shown in the right of Fig. 5(b), SPM-based CIIR process gives us the new reconstruction distance, which

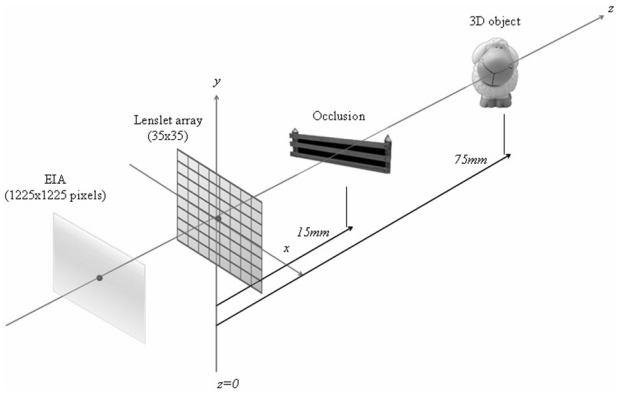

FIG. 6. Experimental setup

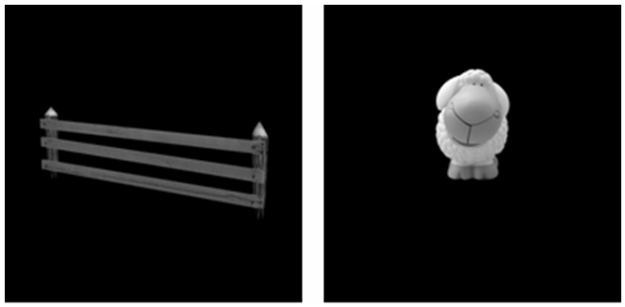

(a) (b)

FIG. 7. Experimental test images (a) Occlusion 'Fence' (b) Target object 'Sheep'

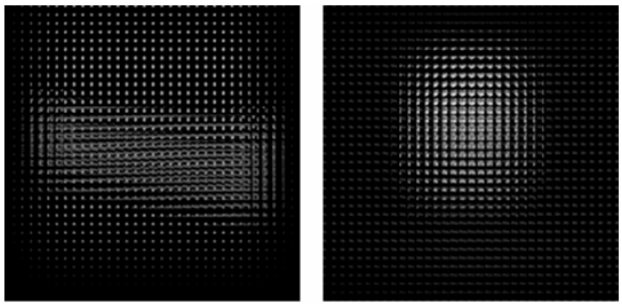

(a) (b)

FIG. 8. (a) Original EIA (b) Depth-reversed EIA

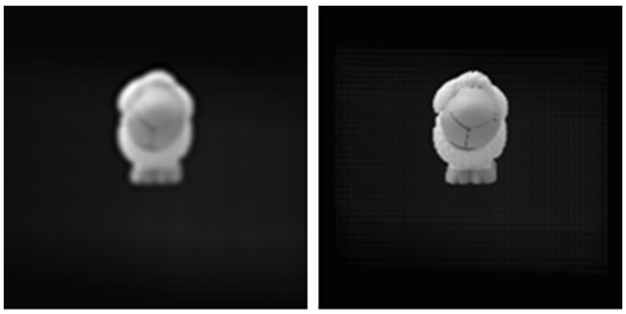

(a) (b)

FIG. 9. Reconstructed plane images (a) With the original EIA (b) With the depth-reversed EIA

is given by

$$z' = d - z = Mg - z \tag{8}$$

This new reconstruction distance allows the 3D object to be reconstructed computationally near to the lenslet array and thus improve the resolution of the reconstructed images.

IV. EXPERIMENTS AND RESULTS

We performed the preliminary experiments to show the usefulness of the proposed method. Throughout all of the experiments, we have adopted the structure as depicted in Fig. 7. Occlusion and 3D object are placed at $z = 15$ mm and $z = 75$ mm, respectively. Then we can obtain the partially occluded object. The size of lenslet array used to record the 3D objects is 35×35. The focal length of the lenslet is $f = 3$ mm. An elemental image consists of 35×35 pixels and then the size of EIA is 1225×1225 pixels.

In the experiment, we performed a few experiments with different pairs of synthesized 3D objects. One of the test object pairs is shown in Fig. 7, which consists of an occlusion 'Fence' and a target object 'Sheep'. The EIA synthesized from these test objects is shown in Fig. 8(a). The EIA was applied with the SPM algorithm to generate a depth-reversed EIA, which is shown in Fig. 8(b).

The depths of both test objects were changed in the depth-reversed EIA. Thus, we need to calculate the depth of target object 'Sheep' before the reconstruction takes place. By using Eq. (8), d is calculated as 105 mm and thus the new distance of the reconstruction plane was obtained as z'=30 mm. The depth-reversed EIA allows the 3D object to be reconstructed virtually near to the lenslet array, which can provide improvement in terms of image quality. In order to make the comparison, we had reconstructed the 3D object as plane image by using the original EIA and depth-reversed EIA, at the distances $z = 75$ mm and $z' = 30$ mm, respectively, as shown in Fig. 9. As can be observed, the plane image reconstructed at the distance nearer to the lenslet array is clearer than the one reconstructed at its initial depth.

For the objective evaluation, we had also adopted peak signal-to-noise ratio (PSNR) as a measurement for image quality, which is defined as

$$PSNR = 10 \log_{10} \frac{255^2}{MSE} \tag{9}$$

and MSE is defined as

$$MSE = \frac{1}{PQ} \sum_{x=1}^{P} \sum_{y=1}^{Q} [R(x,y) - S(x,y)]^2 \tag{10}$$

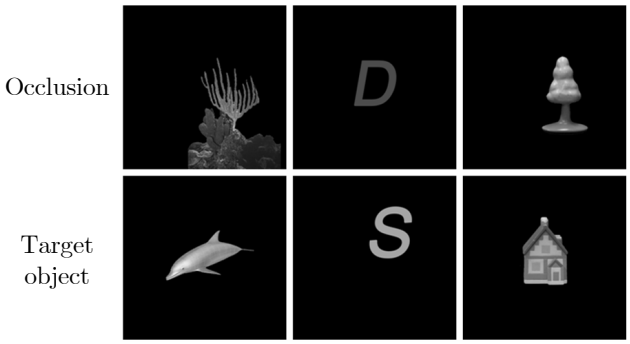

FIG. 10. Experimental test object sets (a) Coral-Dolphin (b) Character 'D' and 'S' (c) Tree-House

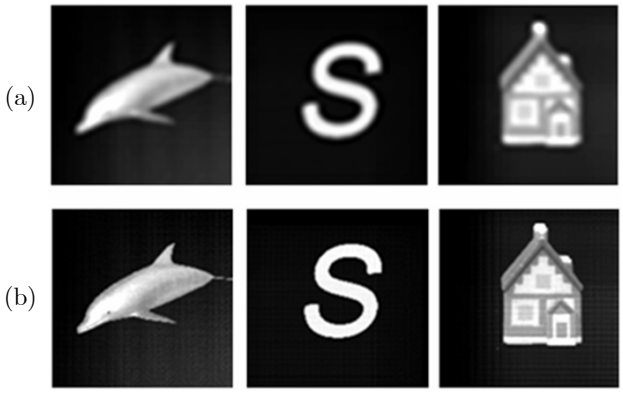

FIG. 11. Reconstructed plane images for test objects shown in Fig. 10 (a) With the original EIA (b) With the depth-reversed EIA

TABLE 1. PSNR results of reconstructed target objects

Object set	PSNR using the conventional CII	PSNR using the SPM-based CII
Fence-Sheep	22.01 dB	22.48 dB
Coral-Dolphin	22.37 dB	24.38 dB
D-S	22.57 dB	23.27 dB
Tree-House	23.81 dB	24.84 dB

where P and Q are the size of reconstructed images in x- and y-direction. $S(x, y)$ and $R(x, y)$ represent the reference image and the reconstructed plane image, respectively.

Figure 10 shows the other test objects pairs used for the experiments. Their reconstructed images are shown in Fig. 11. The PSNR values for all the reconstructed target objects are summarized in Table 1. The PSNR results show the proposed SPM-based CII system achieves better performance than the conventional CII system. The proposed system obtains an average PSNR increment of about 1.05 dB.

V. CONCLUSION

In conclusion, we have presented a SPM-based CII method and applied to the partially occluded 3D object reconstruction to improve the resolution. Since the SPM technique changes the initial depths of the 3D objects, the occluded object located at far distance was able to be computationally reconstructed at the distance near to the lenslet array, which allows the 3D object to be reconstructed with higher resolution. To show the usefulness of the proposed method, we carried out some experiments for several object sets and compared the results with the conventional CII system. As a result, our proposed SPM CII system has obtained an average improvement of about 1.05dB for the test objects used.

REFERENCES

1. A. Stern and B. Javidi, "Three-dimensional image sensing, visualization, and processing using integral imaging," Proc. IEEE **94**, 591-607 (2006).
2. G. Lippmann, "La photographic intergrale," C. R. Acad. Sci. **146**, 446-451 (1908).
3. F. Okano, H. Hoshino, J. Arai, and I. Yuyama, "Real-time pickup method for a three-dimensional image based on integral photography," Appl. Opt. **36**, 1598-1603 (1997).
4. B. Lee, S. Jung, and J.-H. Park, "Viewing-angle-enhanced integral imaging by lens switching," Opt. Lett. **27**, 818-820 (2002).
5. J.-S. Jang and B. Javidi, "Time-multiplexed integral imaging for 3D sensing and display," Optics and Photonics News **15**, 36-43 (2004).
6. H. Arimoto and B. Javidi, "Integral three-dimensional imaging with digital reconstruction," Opt. Lett. **26**, 157-159 (2001).
7. S.-H. Hong, J.-S. Jang, and B. Javidi, "Three-dimensional volumetric object reconstruction using computational integral imaging," Opt. Exp. **12**, 483-491 (2004).
8. S.-H. Hong and B. Javidi, "Improved resolution 3D object reconstruction using computational integral imaging with time multiplexing," Opt. Exp. **12**, 4579-4588 (2004).
9. D.-H. Shin and H. Yoo, "Image quality enhancement in 3D computational integral imaging by use of interpolation methods," Opt. Exp. **15**, 12039-12049 (2007).
10. S. Yeom and B. Javidi, "Photon counting linear discriminant analysis with integral imaging for occluded target recognition," J. Opt. Soc. Korea **12**, 88-92 (2008).
11. D.-H. Shin and H. Yoo, "Scale-variant magnification for computational integral imaging and its application to 3D object correlator," Opt. Exp. **16**, 8855-8867 (2008).
12. M. Martinez-Corral, B. Javidi, R. Martínez-Cuenca, and G. Saavedra, "Formation of real, orthoscopic integral images by smart pixel mapping," Opt. Exp. **13**, 9175-9180 (2005).
13. D.-H. Shin and E.-S. Kim, "Computational integral imaging reconstruction of 3D object using a depth conversion technique," J. Opt. Soc. Korea **12**, 131-135 (2008).
14. B. Javidi, R. Ponce-Díaz, and S. -H. Hong, "Three-dimen-

sional recognition of occluded objects by using computational integral imaging," Opt. Lett. **31**, 1106-1108 (2006).
15. D.-H. Shin, H. Yoo, C.-W. Tan, B-G. Lee, and J.-J. Lee, "Occlusion removal technique for improved recognition of partially occluded 3D objects in computational integral imaging," Opt. Comm. **281**, 4589-4597 (2008).